pH/redox-responsive self-assembling nanoparticles for combinatorial delivery of 5-fluorouracil and methotrexate in colon cancer therapy

H. Guo[a], J. J. Zhang[b], J. H. Liu[a], Y. M. Wang[a], S. J. Fan[a*]
[a]*Research Institute of Medicine and Pharmacy, Qiqihar Medical University, China*
[b]*Department of Neurology, Qiqihar First Hospital, China*

To fulfil the synergistic delivery and on-demand drug release of 5-fluorouracil (5-FU) and methotrexate (MTX) at tumor sites, we innovatively synthesized pH and redox responsive self-assembling nanoparticles based on ZIF-8 frameworks as the 5-FU vehicle decorated with hyaluronic acid-MTX bioconjugates linked with a redox-responsive disulfide bond. The constructed HA-SS-MTX/5-FU@ZIF-8 nanoplatform exhibited monodisperse and spherical shape with a mean hydrodynamic diameter of 161.0nm and loaded about 0.345 g of 5-FU and 0.0508 g of MTX per gram. The preliminary in vitro experiments showed that the as-prepared HA-SS-MTX/5-FU@ZIF-8 nanoparticles (NPs) displayed high inhibiting proliferation and promoting apoptosis performance towards the colon cancer cells.

(Received October 20, 2023; Accepted January 19, 2024)

Keywords: pH/redox sensitive nanoparticles, 5-fluorouracil, Methotrexate, Hyaluronic acid, CD44, ZIF-8

1. Introduction

As early as the fifties of the last century, scientists found that mouse liver cancer cells consumed uracil much faster than normal cells, which means that uracil metabolism is likely to become a target of antimetabolites [1]. Based on this, the antimetabolite drug 5-fluorouracil (5-FU) has also become a broad-spectrum anticancer drug widely used in clinical practice. The anti-tumor mechanism of 5-FU in vivo was mainly contributed by two approaches including the misincorporation of fluoronucleotides into RNA and DNA structures and the inhibition to the physiological effects of thymidylate synthase (TS) [2-5].

Despite the clear mechanism of action, the clinical effect of 5-FU is not ideal. Even in colon cancer treatment that 5-FU has the best efficacy, its response rate is only 10-15% [6]. The primary clinical resistance of 5-FU is rooted in the poor bioavailability because of its rapid degradation catabolized primarily in the liver by dihydropyrimidine dehydrogenase (DPD) to dihydrofluorouracil (DHFU) and loses its efficacy. So, strategies that could inhibit DPD-mediated degradation tend to be effective ways to enhance the efficacy of 5-FU. Plenty of researches were developed, for instance, saturating DPD ahead by the application of a large amount of non-toxic uracil [7, 8], designing prodrugs to protect 5-FU from the degradation by DPD in the liver [9], etc. But these strategies have not improved the response rates in colorectal cancer therapy dramatically.

* Corresponding author: fansongjie@qmu.edu.cn
https://doi.org/10.15251/DJNB.2024.191.161

Thus, we could conclude that simply inhibiting DPD-mediated degradation of 5-FU seemed to be not enough to enhance the antitumor efficacy of 5-FU [10, 11].

Another aspect to improve the antitumor activity of 5-FU is enhancing its inhibition ability to the physiological effects of thymidylate synthase. The combination of methotrexate (MTX) with 5-FU was considered as a potential method [12-14]. MTX itself is an anti-cancer drug with active targeting. Its active targeting stems from the similarity between the molecular structure of MTX and folic acid (FA), resulting in a specific affinity for MTX with the overexpressed folate receptor (Fr) in many cancer cells. MTX is a dihydrofolate reductase (DHFR) inhibitor that inhibits the conversion of dihydrofolate (DHF) to tetrahydrofolate (THF) in the body. THF has important physiological and biochemical functions, such as:(1)THF is an essential raw material for purine biosynthesis; (2)THF is a precursor substance of 5,10-methylenetetrahydrofolate (CH_2THF), and CH_2THF is a carbon donor during uracil deoxynucleotide methylation, which is the only way to synthesize deoxythymidine monophosphate (dTMP) de novo in vivo. MTX can simultaneously inhibit both the purine and thymidine biosynthesis, thereby inhibiting the growth and reproduction of tumor cells. A large number of in vitro [13, 15, 16] and in vivo [17, 18] studies have shown that the pre-administration of MTX can play a good synergistic effect with subsequent 5-FU. Specifically, the inhibition of MTX on the purine biosynthesis increases the levels of phosphoribosyl pyrophosphate (PRPP) in vivo. PRPP is a donor of the phosphoribose group in the conversion of 5-FU to fluorodeoxyuridine monophosphate (FdUMP) catalyzed by orotate phosphoribosyl transferase (OPRT). So, the increased PRPP levels induced by MTX would promote 5-FU ribonucleotides generation and consequently enhance the inhibition ability towards thymidylate synthase and increase 5-FU incorporation into RNA [2]. The antitumor mechanism of MTX and its synergistic mechanism of action on 5-FU can be briefly represented in figure 1.

However, the combination of MTX and 5-FU was not found to be significantly superior to bolus single-agent 5-FU for the treatment of colorectal cancer, no matter in terms of response rate [19] or overall survival [20] which might be derived from the unreasonable application method. Due to the great difference of physical and chemical properties between the two drugs, the amount of 5-FU and MTX at the tumor sites could not achieve the effective dosage at the same time when they were administered in a traditional "cocktail" way.

Based on the above analysis, it is reasonable for us to expect better clinical therapeutic efficacy if we could deliver MTX and 5-FU synergistically to tumor sites in a precise and targeted way and protect 5-FU from being degraded by DPD at the same time. To achieve this goal, we established a pH- and redox-sensitive drug delivery system based on zeolitic imidazolate framework-8 (ZIF-8) as 5-FU vehicles decorated with hyaluronic acid-MTX bioconjugates linked with a redox-responsive disulfide bond though electrostatic interaction to form the HA-SS-MTX/5-FU@ZIF-8 nanoplatform.

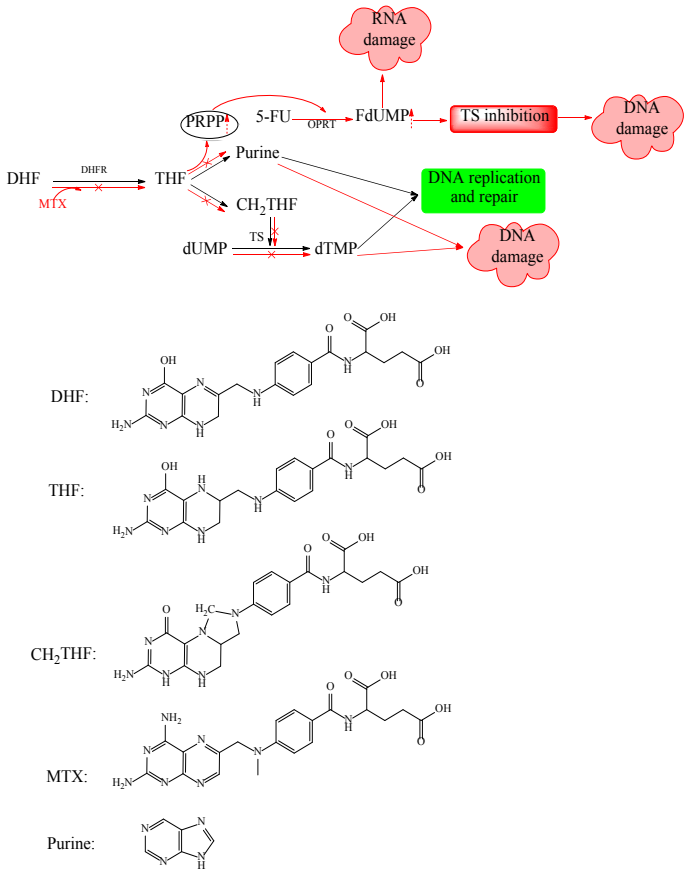

Fig. 1. The antitumor mechanism of MTX and the synergistic mechanism with 5-FU.

ZIF-8 is a kind of hybrid porous solid material with the Zn metal coordinated by the 2-methyl imidazole linker and synthesized by Yaghi and co-workers in 2006 firstly [21]. Benefiting from its unique features (high aqueous stability, good biocompatibility, etc.) especially the pH-sensitivity, ZIF-8 nanoparticles have already been widely employed in cancer therapy as the drug carrier [22-24]. Due to the high metabolic rate of cancer cells, the extracellular microenvironment of cancer tissues tends to be more acidic than the normal tissues. So, loading 5-FU into ZIF-8 nanostructure was expected to be an effective way to achieve the pH-triggered drug release. Moreover, the encapsulation of ZIF-8 keeps 5-FU safely inside and avoid the undesired degradation induced by DPD.

Hyaluronic acid (HA), a linear polysaccharide, is composed of alternating units of a repeating disaccharide, β-1,4-D-glucuronic acid–β-1,3-N-acetyl-D-glucosamine and is widely present in body tissues and extracellular matrix. HA plays a vital role in the process of tumorigenesis and development [25]. In terms of anticancer drugs delivery, HA has attracted much attention as a CD44 ligand targeting moiety. Due to the overexpression of CD44v6 (an isoform of CD44) on the surface of many tumor cells rather than normal cells, HA was expected to delivery drugs to the tumor regions in a targeted manner though the unique ligand-receptor mediated cellular endocytosis effect [25-31].

In this paper we used cystamine (CYS) as a crosslinker to synthesize the HA-SS-MTX conjugates (figure 2). The introduction of disulfide bonds confers redox sensitivity on the entire drug delivery system. Because the disulfide bond is relatively stable in mildly oxidizing and

physiological pH conditions but could be cleaved by metabolic thiols though a reductive cleavage reaction. So, disulfide bonds can be rarely found inside cells due to the abundance of cellular free thiols, especially glutathione (GSH) which is the most abundant thiol-containing small molecule. Furthermore, intracellular GSH concentration is much higher in cancer cells than that in the corresponding normal cells which is beneficial to the rapid cleavage of disulfide linkage inside the cancer cells [32, 33]. Thereby, the HA-SS-MTX conjugates were expected to release MTX at tumor sites with a more effective and precise way and avoid the toxic side effects on normal tissue cells.

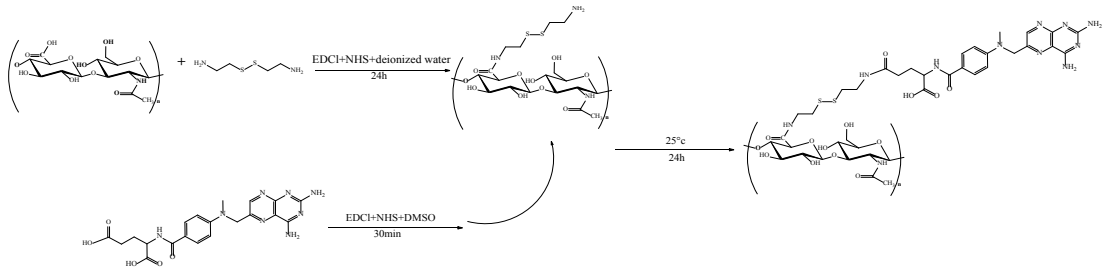

Fig. 2. Synthesis of HA-SS-MTX.

The dual stimulus-response drugs release manner of the HA-SS-MTX/5-FU@ZIF-8 nanoplatform was displayed in Scheme 1. After the rapid endocytosis with the help of the specific binding between HA and CD44, the MTX would release firstly due to the high concentrations of glutathione in tumor cells. Upon endocytosis HA naturally underwent fragmentation to tetrasaccharides by the enzyme hyaluronidase (HAase) in the lysosome [34,35]. Finally, the wrapped 5-FU released from the collapsed ZIF-8 frameworks engendered by the acidic tumor microenvironment. This pH/redox-sensitive and tumor specific drug release system was expected to achieve the combinatorial delivery of 5-FU and MTX and consequently obtain better treatment efficacy.

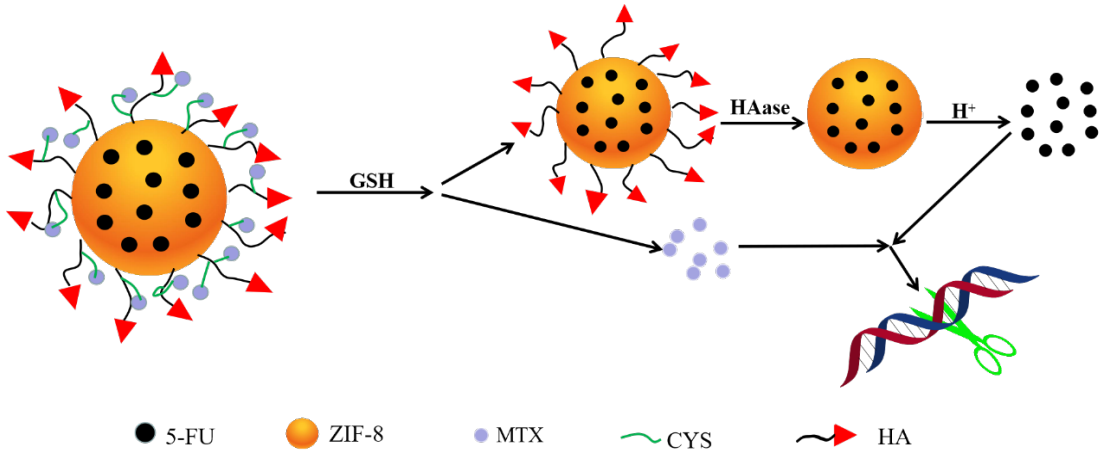

Scheme 1. Schematic representations of the stimulus-response release of the HA-SS-MTX/5-FU@ZIF-8 nanoplatform.

2. Experimental section

2.1. Material

All the reagents used here were analytically pure. $Zn(NO_3)_2$•$6H_2O$ (99%) was obtained from Tianjin reagent, Co., Ltd. 2-methylimidazolate (98%), and 5-FU (99%) were provided by aladdin reagent, Co., Ltd, Shanghai. Hyaluronic acid (100-150 kDa), MTX (99%), 1-hydroxypyrrolidine-2,5dione (NHS,99.8%), 1-ethyl-3-[3-dimethylaminopropyl]carbodiimide hydrochloride (EDCl, 98.5%) and cystamine dihydrochloride (CYS) were purchased from Shanghai Macklin Biochemical Co., Ltd. Methanol (99.9%, HPLC Grade) was acquired from Dikema Technology Co., Ltd. DMSO were obtain from Biyuntian Biotechnology Co., Ltd.

2.2. Synthesis

2.2.1. Synthesis of 5-FU@ZIF-8

The synthesis of 5-FU@ZIF-8 and the method to gain the amount of absorbed 5-FU in 5-FU@ZIF-8 have been described in detail in our earlier paper [36] and the relevant content would not be restated here.

2.2.2. Synthesis of HA-SS and HA-SS-MTX

The HA-SS-MTX prodrug was prepared according to previous described literature with very little modification [32]. Briefly, HA (100mg, 0.264mmol), EDC·HCl (151mg, 0.792mmol), and NHS (91.1mg, 0.792mmol) were dissolved in 5ml deionized water and stirred for 30min under 25℃ to activate the carboxyl group of HA molecules, and then CYS (101.8mg, 0.452mmol) was added. The reaction mixture was stirred for 24h. Afterwards, the reaction mixture was transferred to a dialysis bag (Mw cutoff 3500) and dialyzed exhaustively against deionized water. Finally, the solution in the dialysis bag was flash frozen and lyophilized to get a white and cotton-like solid for later use.

The as-prepared HA-SS was dissolved in 3 mL of formamide under mild heating condition and cooled down to 25 °C and then 2ml DMSO was added forming the solution 1. MTX (60mg, 0.132mmol), EDC·HCl (60.8mg, 0.317mmol), and NHS (36.5mg, 0.317mmol) were dissolved in 5ml DMSO and stirred for 30min under 25℃ to activate the carboxyl group of MTX molecules. Then solution 1 was added dropwise under continuous stirring. The reaction mixture was stirred for 24h under 25℃. The reaction products were purified by extensive dialysis against deionized water for three days using a dialysis bag (Mw cut-off of 3500 Da). After lyophilization, we obtained the yellow and flocculent HA-SS-MTX bioconjugates. All the dialysate was collected and measured by using UV-vis absorption spectra at 388 nm to evaluate the unlinked amount of MTX based on the calibration curve (figure 3). Then the weight of linked MTX was obtained by performing the subtraction of the amounts of the initial and unlinked amount of MTX. Finally, the mass fraction of MTX in HA-SS-MTX conjugates (W_1 %) could be obtained.

2.2.3. Synthesis of HA-SS-MTX/5-FU@ZIF-8

HA-SS-MTX (0.019g) and 5-FU@ZIF-8 (0.059) g were dispersed in 8ml deionized water separately. Then 5-FU@ZIF-8 solution was added to HA-SS-MTX solution dropwise under ultrasonication for 30 min and the reaction mixture was agitated vigorously at room temperature for 24 h. The product was collected by centrifugation at 14000 rpm for 20 min. Afterwards the

sediment is redispersed into a small amount of water and freeze-dried. The loading amount of MTX was quantified by the equation: $[(m_2-m_1) \times W_1\%]/m_2$. In this equation, m_1 and m_2 refer to the mass of initial 5-FU@ZIF-8 and the final HA-SS-MTX/5-FU@ZIF-8 respectively.

2.3. Cell culture

Human colonic carcinoma cell line HT29 were cultivated in Dulbecco's Modified Eagles's Medium (DMEM, Gibco) supplemented with 10% (v/v) fetal bovine serum (FBS, Weishente bioreagent Co., Zhejiang) and penicillin/streptomycin (100 $U \cdot mL^{-1}$ and 100 $g \cdot mL^{-1}$, respectively, Gibco) and placed in a humidified atmosphere at 37℃with 5% CO_2.

2.4. In vitro cytotoxicity

The cell viabilities were evaluated by the standard 3-(4,5-dimethylthiazol-2-yl)-2,5-diphenyltetrazolium bromide (MTT) assay. Firstly, HT29 cells were cultured into 96 well plates with a density of 5×10^3 cells per well in 100μl of media and grown overnight. Then the cells were incubated for 48 h with different nanoparticles concentrations (5-FU, MTX, 5-FU+MTX, and HA-SS-MTX/5-FU@ZIF-8 NPs). After that, cells were incubated in media of MTT (20μl, 5 $mg \cdot mL^{-1}$) for 4 h. Subsequently, the 96 well plates were centrifuged at 1500 rpm for 10 min to collect the precipitated formazan violet crystals. These formazan violet crystals were dissolved in 150μl DMSO to form clear purple solutions which were detected by a microplate reader (Tecan Safire2, Switzerland) at 490 nm.

The live/dead cell staining assay was also conducted to visually present the in vitro cytotoxicity of these as-prepared materials. Briefly, the HT29 cells were seeded in 6-well plates with a density of 5×10^5 cells per well and incubated with pure 5-FU, MTX, 5-FU+MTX and HA-MTX/5-FU@ZIF-8 NPs for 24 h. Then the culture medium was discarded and fresh medium containing calcein AM and PI was added for observation via a laser-scanning confocal microscopy.

The ability of inducing HT29 cell apoptosis of these materials (pure 5-FU, MTX, 5-FU+MTX and HA-MTX/5-FU@ZIF-8 NPs) was evaluated by flow cytometry. The HT29 cells were treated with these materials for 24 h. Following the standard operating procedures of the apoptosis assays kit (Annexin V-FITC/PI), the cell apoptosis was detected by flow cytometer.

2.5. Characterizations

X-ray diffffraction (XRD) patterns were collected by a Siemens D5005 diffractometer using Cu ka radiation (λ = 1.5418 Å). The morphologies of the samples were monitored with FEI Tecnai G2 F20 S-TWIN transmission electron microscope (TEM). The TGA was performed under air flow at a heating rate of 1℃/min in the range of 25-900℃ with a Perkin-Elmer TGA thermogravimetric analyzer. Vibrational spectra were obtained by Fourier transform infrared spectroscopy (FTIR) analysis on a Nicolet Impact 410 FTIR spectrometer to investigate the existence of functional groups in these samples at 25℃ with the KBr technique at a resolution of 4 cm^{-1} and wavenumber range of 4000-400cm^{-1}. The UV-Vis absorption spectra were determined by a UV-759 spectrophotometer. NMR analysis was conducted on a AVANCE NEO 600 MHz spectrometer using D_2O containing 0.25 mol/L NaOD as solvent. The hydrodynamic diameters, PDI and zeta-potential values of all the samples were measured using the dynamic light scattering (DLS) and electrophoretic light scattering (ELS) techniques on a Nicomp 380ZLS (PSS, USA).

3. Results and discussions

3.1. Characterizations of samples

The ^{13}C NMR spectra was applied to identified the formation of the HA-SS-MTX bioconjugates (figure 4). We could see that four characteristic CYS peaks appeared in the spectrum of the HA-SS conjugates at δ 37.9ppm, 39.1ppm, 40.5ppm and 43.7 ppm (figure 4b). Meanwhile, the peak at 181.8ppm tended to be ascribed to the new amide carbon (carbon number 5 in the inserted structural diagram of HA-SS). After conjugation with MTX, four characteristic MTX peaks (111.6ppm, 129.2ppm, 146.7ppm and 155.5ppm) and two characteristic signals of CYS (40.4ppm and 43.7 ppm) were observed clearly in the spectra of HA-SS-MTX (figure 4d). Furthermore, a new signal generated at 171.0 ppm was expected to be attributable to the amide carbon (carbon number 1 in the inserted structural diagram of HA-SS-MTX). All these above signals demonstrated the successful grafting of MTX to the skeleton of HA through the redox-responsive linker (CYS).

From figure 5a we could see that after the electrostatic interaction with 5-FU@ZIF-8 NPs, the HA-SS-MTX aqueous solution color changed from dark yellow to light yellow. In addition, a dramatical change of zeta potential in deionized water was observed from +18.83 mV (5-FU@ZIF-8) inversely to -27.84 mV (HA-SS-MTX/5-FU@ZIF-8) due to the coating of HA-SS-MTX (-36.49 mV) (figure 5b). Obviously, these results demonstrated that the negatively charged HA-SS-MTX was introduced as a layer to the outside surface of 5-FU@ZIF-8 NPs. According to the size distribution result (figure 5c), the diameter of HA-SS-MTX/5-FU@ZIF-8 NPs was about 161.0nm with low polydispersity index (PDI; 0.288) indicating excellent uniformity and dispersibility.

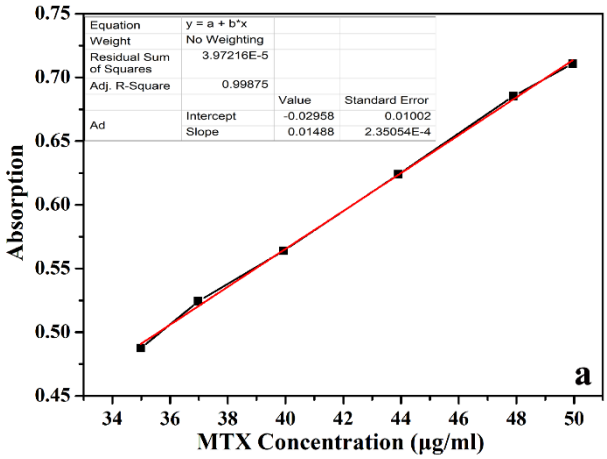

Fig. 3. The standard curve for MTX solutions detected at 388nm by UV-vis spectrophotometer.

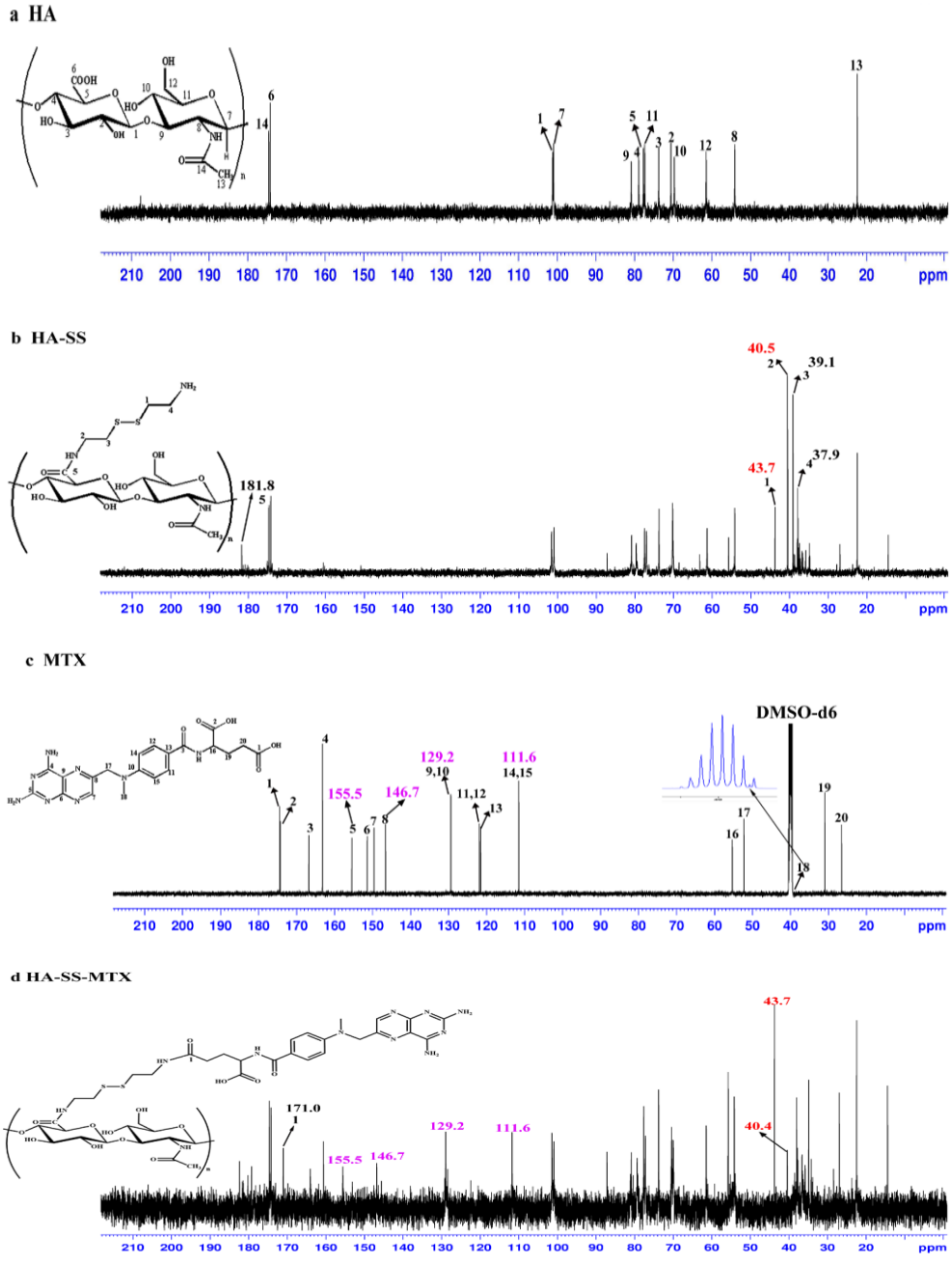

Fig. 4. ^{13}C NMR spectra of HA(a); HA-SS (b); MTX (c); HA-SS-MTX (d).

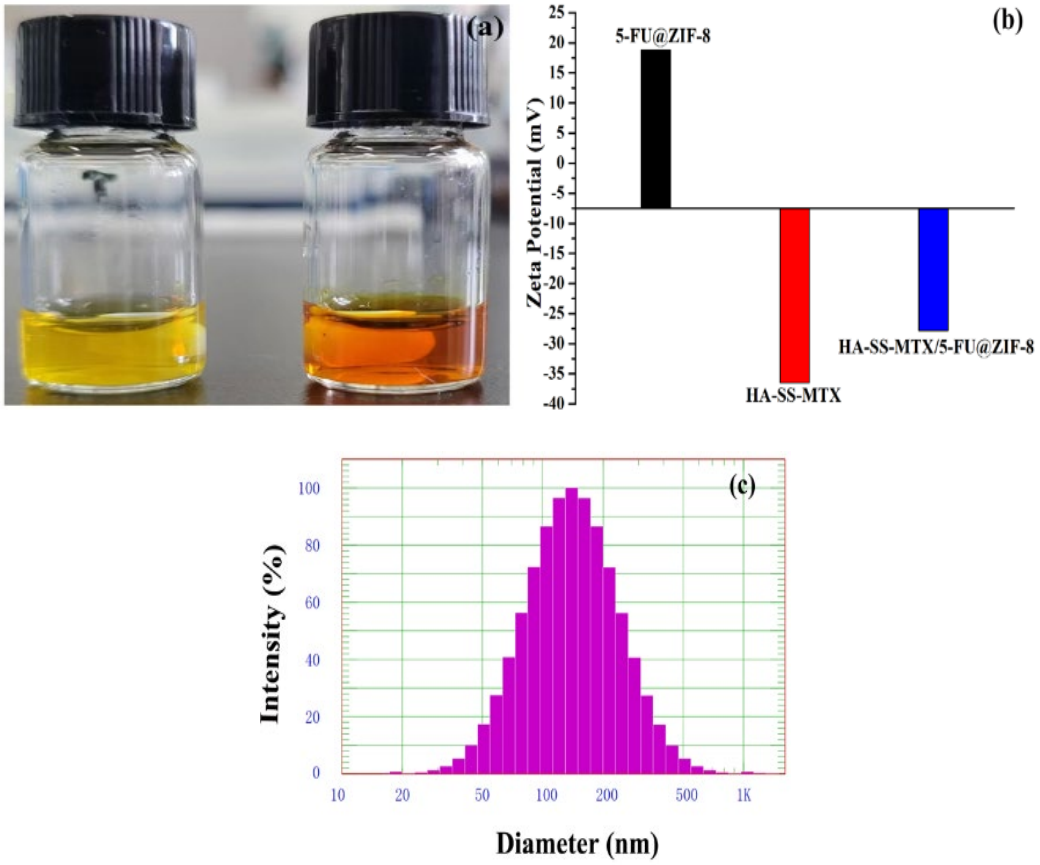

Fig. 5. (a) Optical images of HA-SS-MTX aqueous solutions before (right) and after (left) electrostatic interaction with 5-FU@ZIF-8 NPs; (b) Zeta potentials of 5-FU@ZIF-8, HA-SS-MTX and HA-SS-MTX/5-FU@ZIF-8 in deionized water. (c) The size distribution of HA-SS-MTX/5-FU@ZIF-8 NPs in deionized water.

In addition, after the coating of the HA-SS-MTX bioconjugates most of the characteristic peaks of HA-SS-MTX/5-FU@ZIF-8 matched well with the simulated ZIF-8 diffractogram indicating the good preservation of the crystallinity of the ZIF-8 network (figure 6a). Meanwhile, due to the external amorphous polymer coating, the XRD signal intensity of HA-SS-MTX/5-FU@ZIF-8 become obviously weakened.

From the fourier transformed infrared spectroscopy (FTIR, figure 6b), we could see two newly generated peaks in the FT-IR spectroscopy of HA-SS at 3085cm^{-1} and 1731cm^{-1} compared with HA which were ascribed to the stretching vibration of N-H and NC=O respectively indicating the formation of the amide bond between HA and CYS. Besides the above two stretching vibration signals, four characteristic peaks of MTX were also observed in the FT-IR spectroscopy of HA-SS-MTX at 1546cm^{-1}, 1205 cm^{-1}, 828 cm^{-1} and 776 cm^{-1} demonstrating the successful grafting of MTX to the skeleton of HA through the redox-responsive linker (CYS).

The thermogravimetric analysis was used to evaluate the stability and thermal decomposition of the samples and the results were displayed in figure 6c. As we have described in our earlier work, pure ZIF-8 frameworks could keep stable until 580℃ and as for 5-FU@ZIF-8, the weight loss temperature advanced to about 300℃ due to the decomposition of 5-FU [35]. In case of HA-SS-MTX/5-FU@ZIF-8, the more thermally unstable polymer coating leaded the first weight loss to advance to about 208℃ which was consistent with that of HA-SS-MTX.

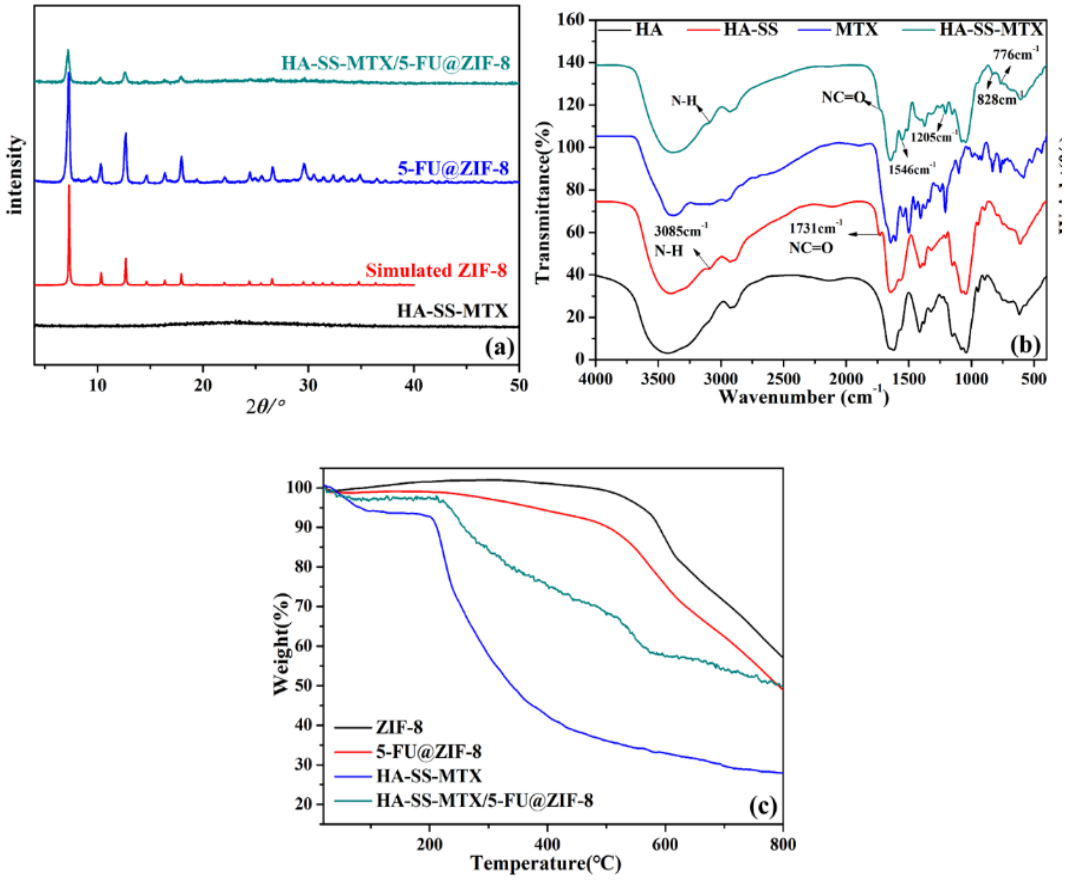

Fig. 6. (a) XRD patterns of simulated ZIF-8, 5-FU@ZIF-8, HA-SS-MTX and HA-SS-MTX/5-FU@ZIF-8; (b) FT-IR spectra of HA, HA-SS, MTX and HA-SS-MTX; (c) TG curve of ZIF-8, 5-FU@ZIF-8, HA-SS-MTX and HA-SS-MTX/5-FU@ZIF-8.

The micromorphology of 5-FU@ZIF-8 and HA-SS-MTX/5-FU@ZIF-8 NPs was displayed in figure 7a and b. Overall, the as-prepared HA-SS-MTX/5-FU@ZIF-8 NPs is monodisperse with uniform morphology. The mean diameter of HA-SS-MTX/5-FU@ZIF-8 NPs is in the range of 50-80 nm. Overall, after the polymer coating, no obvious change in particles size took place but a pale shell formed on the outer surface of 5- FU@ZIF-8 nanoparticles could be observed obviously. Meanwhile, dramatical changes of the macroscopical morphology appeared from a white powdery solid (5-FU@ZIF-8) to a yellowish and fluffy material (HA-SS-MTX/5-FU@ZIF-8, figure 7c). The features of size and spherical shape might facilitate the HA-SS-MTX/5-FU@ZIF-8 NPs endocytosis and the enhanced penetration and retention effect.

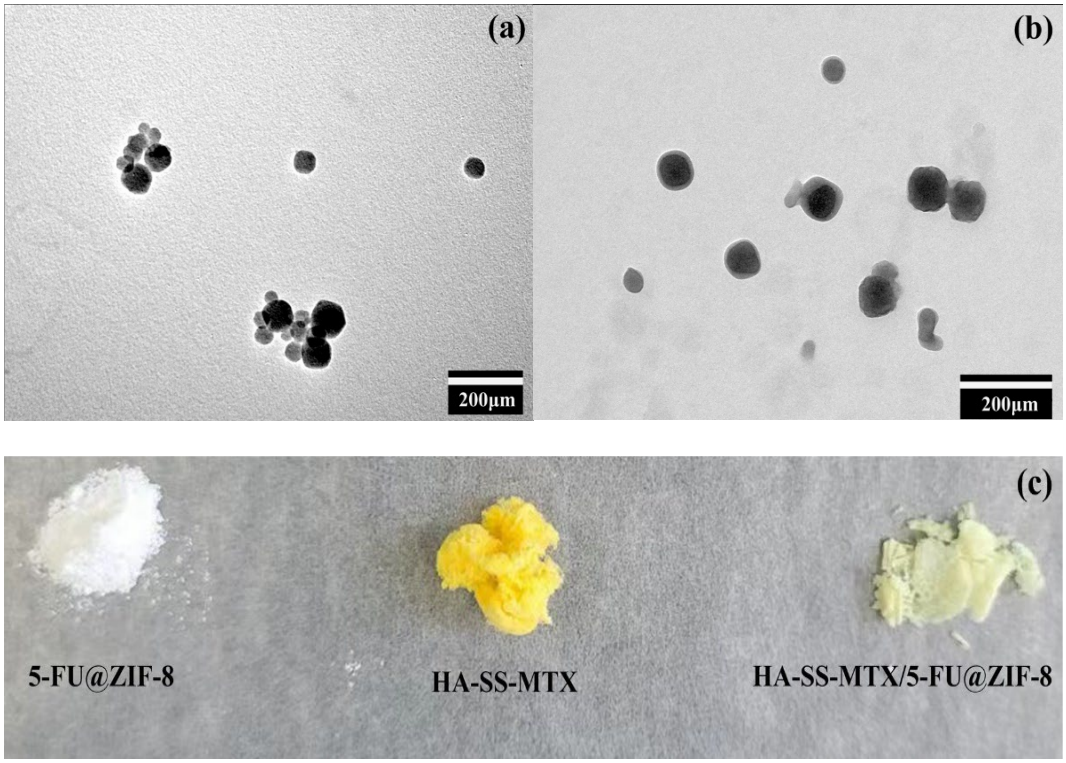

Fig. 7. TEM images of: 5- FU@ZIF-8 (a); HA-SS-MTX/5- FU@ZIF-8 (b); Optical images of these samples (c).

3.2. Drugs loading efficiency and redox-responsive drug release

The per gram of as-prepared HA-SS-MTX/5-FU@ZIF-8 NPs load about 0.345 g of 5-FU and 0.0508 g of MTX. Certainly, a higher MTX loading could be obtained but it has been found that the degree of substitution (DS) (ratio between the number of substituted reactive group (the carboxylate groups in our paper) and the number of repeating disaccharide units of the polysaccharide) above 25% would decrease the HA's ability to target CD44 receptors and change the HA's overall charge [31]. That is to say, the the drug loading and the HA's targeting properties are contradictory and restrictive. A great number of experimental studies are essential to determine the optimal DS value to gain the best therapy effect. In this paper the substitution degree of HA was about 31% and the mass fraction of MTX in HA-SS-MTX conjugates (W_1 %) was about 23.9%.

To confirm the stimulus-response release of MTX induced by GSH, the drug release behavior was determined by a dialysis method in PBS buffer solution and the amount of MTX released was measured by a UV-vis spectrophotometer (figure 8). We could see that there was no obvious adsorption peak in the HA-SS spectrum. The two characteristic peaks of MTX appeared at 299nm and 388nm. As for HA-SS-MTX, we could detect the free MTX signals in the dialysis solution with 10mM GYS but no obvious adsorption peaks were observed in the dialysis solution without GYS after the same dialysis time (about 6 hours). These results indicated that MTX molecules could be released from the HA-SS-MTX bioconjugates after the cleavage of disulfide bonds induced by the simulation of GSH. The pH responsive drug release of 5-FU@ZIF-8 NPs has been evaluated in our earlier work (figure S1) [35].

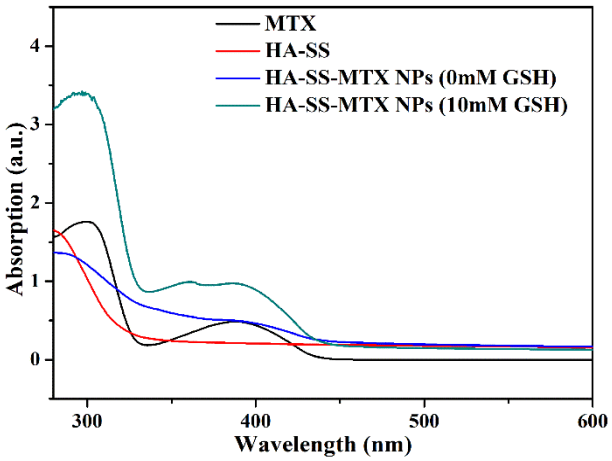

Fig. 8. UV-Vis absorption spectra of MTX, HA-SS and HA-SS-MTX in PBS with different concentration of GSH.

3.3. In Vitro Cytotoxicity Studies

The cytotoxicity of as-prepared HA-SS-MTX/5-FU@ZIF-8 NPs towards HT29 cells, folate and CD44 receptors-overexpressing cancer cells, were determined by the MTT assay and the data were used to obtain the IC_{50} values by the dose-effect relationship fitting (figure 9a). For comparison, the free 5-FU, free MTX, and free 5-FU+MTX mixture (the ratio of the two drugs were the same with that of the HA-SS-MTX/5-FU@ZIF-8 nanoparticles) were also studied at a series of concentrations. As shown in figure 9a, both the two free drug solutions, 5-FU+MTX and HA-SS-MTX/5-FU@ZIF-8 NPs showed a concentration-dependent cell-killing ability. In addition, no significant cytotoxicity of the drug vehicles ZIF-8 material was observed indicating that ZIF-8 NPs did not impact the mechanism of pharmacological action of both small molecular drugs 5-FU and MTX (figure S2). The IC_{50} value of HA-SS-MTX/5-FU@ZIF-8 (13.24μg/mL) nearly dropped to one seventh of the the single 5-FU (91.42μg/mL) and one sixth of pure MTX (79.89μg/mL) indicating that the combination of the two drug indeed inhibit the proliferation of the cancer cells. Furthermore, with the help of the ligand-receptor mediated endocytosis contributed by HA, HA-SS-MTX/5-FU@ZIF-8 NPs exhibited much higher cytotoxicity compared with the simple 5-FU+MTX mixture (IC_{50}=48.14μg/mL). From the cells apoptosis results (figure 9d), we could see that all the four groups tended to migrate from live cells status to early and late apoptosis compared with the control group confirming an apoptosis-activated cell death pathway. Moreover, the quantitative analysis of percent apoptotic cells (figure. 9e) showed that the group treated with HA-SS-MTX/5-FU@ZIF-8 NPs possessed the highest cell apoptotic percentage (20.69%) with significant statistical differences with 5-FU+MTX group confirming that the dual stimulus-response multi-drug delivery nanoplatform could fulfil the effective combination of MTX and 5-FU and subsequently obtain better antitumor efficiency. The results of live/dead cell staining assays and the corresponding fluorescent quantitative analysis (figure. 9b and c) also coincide with the above cytotoxicity tests and cells apoptosis results.

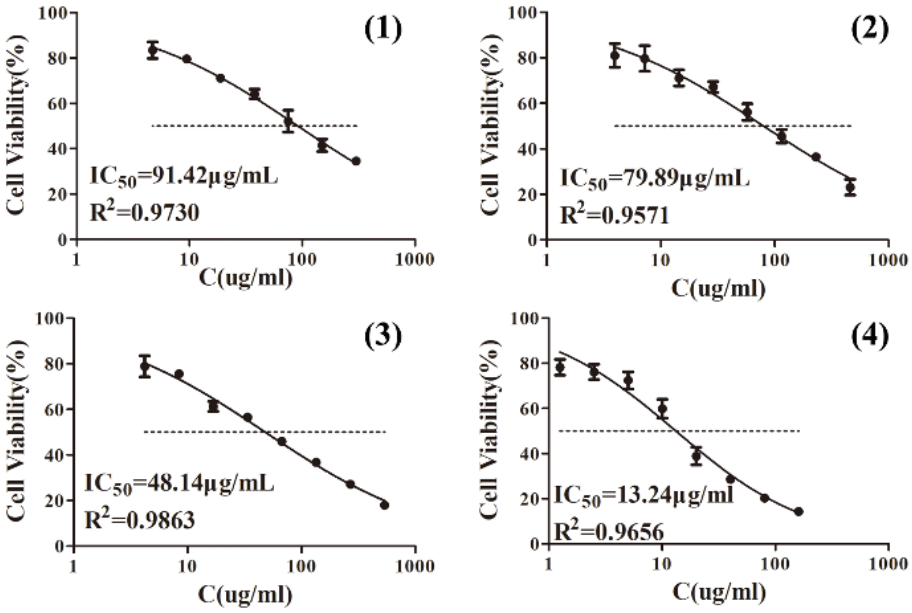

(a)

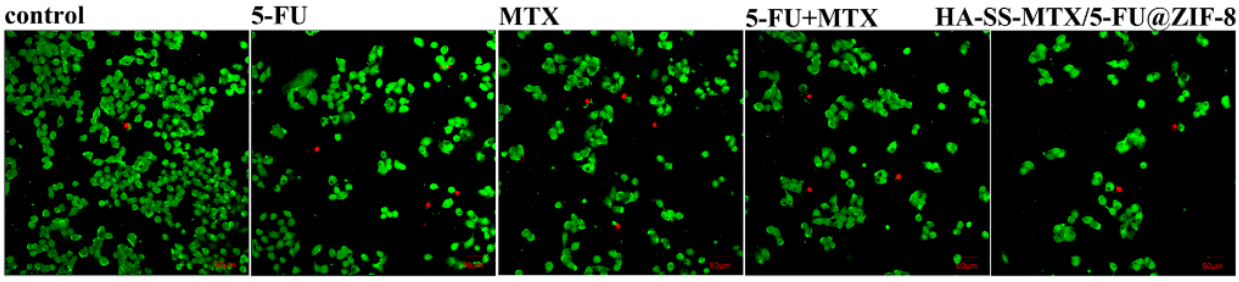

(b)

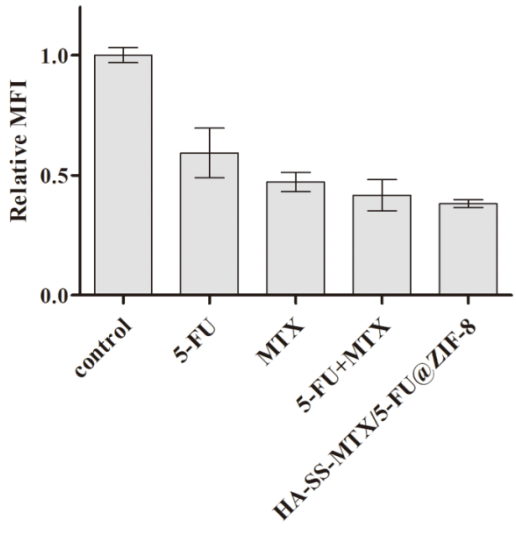

(c)

Fig. 9.1. Cell viability of HT29 after 24 h incubation with different concentrations of 5-FU, MTX, 5-FU+MTX, HA-SS-MTX/5-FU@ZIF-8 (from 1 to 4), and the calculated IC50 values

(a) CLSM images of HT29 cells after incubation with these samples (24 h), dyed with calcein AM/ PI

(b) the corresponding fluorescent quantitative analysis

(c) Annexin V-FITC/PI double-staining to analyze the HT29 cells apoptosis treated with these samples (24 h) by flow cytometry

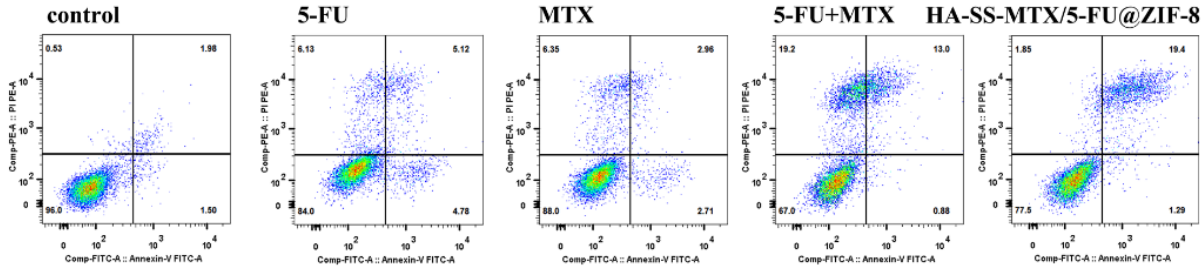

(d)

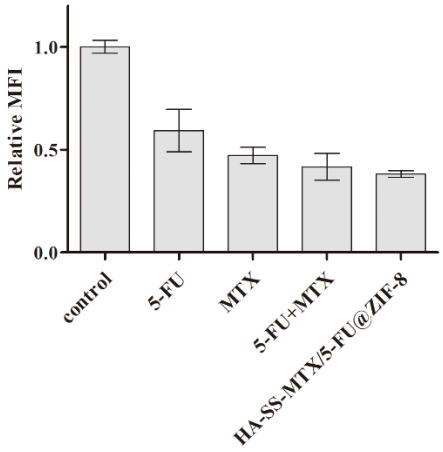

(e)

Fig. 9.2. Cell viability of HT29 after 24 h incubation with different concentrations of 5-FU, MTX, 5-FU+MTX, HA-SS-MTX/5-FU@ZIF-8 (from 1 to 4), and the calculated IC50 values
(d) The quantitative analysis of apoptotic cells percent
*(e). The unmarked asterisk is the result of comparison with the control group, ***P < 0.001.*

4. Conclusion

In this paper we innovatively combined the CD44 receptors mediated targeting ability of HA, the redox-responsive disulfide bond and the pH-sensitive dissolution property of ZIF-8 frameworks to fabricate a dual pH/Redox-responsive drug delivery system (HA-SS-MTX/5-FU@ZIF-8) to achieve the combinatorial delivery and on-demand drug release of 5-FU and MTX at the tumor sites. Preliminary in vitro experiments showed that the as-prepared HA-SS-MTX/5-FU@ZIF-8 NPs exhibited high inhibiting proliferation and promoting apoptosis performance towards the colon cancer cells indicating that the nanoplatforms indeed enhanced the synergistic anticancer effect of 5-FU and MTX. Taken together with the precise targeting, controlled release, and high cytotoxicity, these creative HA-SS-MTX/5-FU@ZIF-8 NPs hold a promising prospect in clinical application. More importantly, due to the facile yet versatile procedure it is potential to expand this strategy to other multi-drug synergistic combination systems and provide an appealing alternative therapy against cancer.

Acknowledgements

We are grateful to the financial support from the Basic Scientific Research Project of Heilongjiang Province in 2022, China (grant no. 2022-KYYWF-0812) and the Joint Guidance

project of Qiqihar Science and Technology Plan in 2022, China (grant no. LSFGG-2022047) and the Joint Guidance project of Qiqihar Science and Technology Plan in 2023, China (grant no. LSFGG-2023029) and General Fund project of Qiqihar Academy of Medical Sciences, China (grant no. QMSI2022M-06).

References

[1] R.J. Rutman, A. Cantarow, K.E. Paschkis, Cancer research 14(2), 119 (1954).

[2] D.B. Longley, D.P. Harkin, P.G. Nature Reviews Cancer 3(5), 330 (2003); https://doi.org/10.1038/nrc1074

[3] J. Boyer, P.J. Maxwell, D.B. Longley, P.G. Johnston, Anticancer Res 24, 417 (2004)

[4] K. Ghoshal, S.T. Jacob, Cancer research 54(3), 632 (1994).

[5] R.D. Ladner, Current Protein & Peptide Science 2(4), 361 (2001); https://doi.org/10.2174/1389203013380991

[6] P.G. Johnston, S. Kaye, Anticancer Drugs 12(8), 639(2001); https://doi.org/10.1097/00001813-200109000-00001

[7] V. Sharma, S.K. Gupta, M. Verma, Cancer Chemotherapy and Pharmacology 84(6), 1157 (2019); https://doi.org/10.1007/s00280-019-03936-w

[8] R. Stec, L. Bodnar, M. Smoter, M. Maczewski, C. Szczylik, Oncology Letters 2(1), 3 (2011); https://doi.org/10.3892/ol.2010.212

[9] V.J. Rani, A. Raghavendra, P. Kishore, Y.N. Kumar, K.H. Kumar, K. Jagadeeswarareddy, European Journal of Medicinal Chemistry 54, 690(2012); https://doi.org/10.1016/j.ejmech.2012.06.023

[10] D.C. Forouzesh, B.A. Beaupre, A. Butrin, Z. Wawrzak, D.L. Liu, G.R. Moran, Biochemistry 60(14), 1120 (2021); https://doi.org/10.1021/acs.biochem.1c00096

[11] H.J. Schmoll, Anti-Cancer Drugs 14(9), 695(2003); https://doi.org/10.1097/00001813-200306002-00007

[12] V.S. Kushwaha, S. Gupta, N. Husain, H. Khan, M.P.S. Negi, N. Jamal, A. Ghatak, Gefitinib, Cancer Biology & Therapy 16(2), 346 (2015); https://doi.org/10.4161/15384047.2014.961881

[13] A.M. Mohammed, S.K. Osman, K.I. Saleh, A.M. Samy, Aaps Pharmscitech 21(4),131 (2020); https://doi.org/10.1208/s12249-020-01672-6

[14] J. Gao, X.B. Li, J.W. Chen, W.D. Gong, K. Yue, Z.Q. Wu, Medicine 97(5), 9722 (2018); https://doi.org/10.1097/MD.0000000000009722

[15] M.B. Singh, V.K. Vishvakarma, A.A. Lal, R. Chandra, P. Jain, P. Singh, Journal of the Indian Chemical Society 99(12), (2022); https://doi.org/10.1016/j.jics.2022.100790

[16] K.J. Sohn, F. Smirnakis, D.N. Moskovitz, P. Novakovic, Z. Yates, M. Lucock, R. Croxford, Y.I. Kim , Gut 53(12), 1825 (2004); https://doi.org/10.1136/gut.2004.042713

[17] S.E. Rivkin, S.J. Green, D. Lew, J.J. Costanzi, J.W. Athens, C.K. Osborne, C.B. Vaughn, S. Martino, Cancer 97(1), 21 (2003); https://doi.org/10.1002/cncr.10982

[18] J.M. Pesic, D.A. Donat, J.D. Trifunovic, L.B. Muzikravic, T.M. Pesic, D.D. Donat, Annals of Oncology 17, 84(2006).

[19] A. Sobrero, G. Frassineti, A. Falcone, L. Dogliotti, R. Rosso, F.D. Costanzo, P. Bruzzi, Intacc, British Journal of Cancer 92(1), 24 (2005); https://doi.org/10.1038/sj.bjc.6602276

[20] Y. Matsumura, K. Haruyama, T. Hamaguchi, K. Shirao, K. Muro, Y. Yamada, Y. Shimada, K. Sugano, Japanese Journal of Clinical Oncology 32(1), 9 (2002).

[21] K.S. Park, Z. Ni, A.P. Côté, J.Y. Choi, R. Huang, F.J. Uribe-Romo, H.K. Chae, M. O'Keeffe, O.M. Yaghi, Proceedings of the National Academy of Sciences 103(27), 10186 (2006); https://doi.org/10.1073/pnas.0602439103

[22] J.S.F. Silva, J.Y.R. Silva, G.F. de Sa, S.S. Araujo, M.A. Gomes Filho, C.M. Ronconi, T.C. Santos, S.A. Junior, Acs Omega 3(9), 12147 (2018); https://doi.org/10.1021/acsomega.8b01067

[23] C.-Y. Sun, C. Qin, X.-L. Wang, G.-S. Yang, K.-Z. Shao, Y.-Q. Lan, Z.-M. Su, P. Huang, C.-G. Wang, E.-B. Wang, Dalton Transactions 41(23), 6906 (2012); https://doi.org/10.1039/c2dt30357d

[24] R. Ettlinger, N. Moreno, D. Volkmer, K. Kerl, H. Bunzen, Chemistry European Journal. 25(57), 13189 (2019); https://doi.org/10.1002/chem.201902599

[25] J.A. Burdick, G.D. Prestwich, Advanced Materials 23(12), H41(2011); https://doi.org/10.1002/adma.201003963

[26] A. Banzato, S. Bobisse, M. Rondina, D. Renier, F. Bettella, G. Esposito, L. Quintieri, L. Melendez-Alafort, U. Mazzi, P. Zanovello, Clinical Cancer Research An Official Journal of the American Association for Cancer Research 14(11), 3598 (2008); https://doi.org/10.1158/1078-0432.CCR-07-2019

[27] Z. Xu, W.Z. And, Z. Yin, Archiv Der Pharmazie 347(4), 240 (2014); https://doi.org/10.1002/ardp.201300177

[28] S. Cai, Y.M. Xie, T.R. Bagby, M.S. Cohen, M.L, Journal of Surgical Research 147(2), 247 (2008); https://doi.org/10.1016/j.jss.2008.02.048

[29] Gurav, Deepanjali, D, Shinde, Vaishali, S., Khan, Ayesha, Kulkarni, Anuja, Colloids & Surfaces B Biointerfaces 143, 352 (2016); https://doi.org/10.1016/j.colsurfb.2016.03.049

[30] Q.Q. Sun, H.T. Bi, Z. Wang, C.X. Li, X.W. Wang, J.T. Xu, H. Zhu, R.X. Zhao, F. He, S.L. Gai, P.P. Yang, Biomaterials 223, 11(2019); https://doi.org/10.1016/j.biomaterials.2019.119473

[31] F. Dosio, S. Arpicco, B. Stella, E. Fattal, Advanced Drug Delivery Reviews 97, 204 (2016); https://doi.org/10.1016/j.addr.2015.11.011

[32] Y.B. Zhang, Y. Li, H.N. Tian, Q.X. Zhu, F.F. Wang, Z.X. Fan, S. Zhou, X.W. Wang, L.Y. Xie, Z.Q. Hou, Molecular Pharmaceutics 16(7), 3133 (2019); https://doi.org/10.1021/acs.molpharmaceut.9b00359

[33] M.H. Lee, Z. Yang, C.W. Lim, Y.H. Lee, S. Dongbang, C. Kang, J.S. Kim, Chemical Reviews 113(7), 5071(2013); https://doi.org/10.1021/cr300358b

[34] O.P. Oommen, J. Garousi, M.S. And, O.P. Varghese, Macromolecular Bioscience 14(3), 327 (2014); https://doi.org/10.1002/mabi.201300383

[35] Guo, H., L. F., L. D., H. L. H., W. Q. Y., S. J. F., Digest Journal of Nanomaterials and Biostructures 2022, 17 (4), pp. 1399-1415; https://doi.org/10.15251/DJNB.2022.174.1399

[36] H. Guo, S. Fan, J. Liu, Y. Wang, Inorganic Chemistry Communications 141, 109616 (2022); https://doi.org/10.1016/j.inoche.2022.109616